X-59 Sonic Boom Test Results from the NASA Glenn 8- by 6-Foot Supersonic Wind Tunnel

Donald A. Durston[1]
NASA Ames Research Center, Moffett Field, California 94035

John D. Wolter[2]
NASA Glenn Research Center, Cleveland, Ohio 44135

Patrick R. Shea,[3] Courtney S. Winski,[4] Alaa A. Elmiligui,[5] Sarah L. Langston,[6]
Michael D. Bozeman,[7] Melissa B. Carter[8]
NASA Langley Research Center, Hampton, Virginia 23681

Christopher A. Bellido[9]
Lockheed Martin Corporation, Palmdale, California 93599

A wind tunnel test was conducted to investigate near-field sonic boom pressure signatures of the X-59 Low-Boom Flight Demonstrator aircraft. A 1.62%-scale model of the aircraft was fabricated for the wind tunnel test, which took place in the NASA Glenn 8- by 6-Foot Supersonic Wind Tunnel in September and October 2021. The model had provisions for being mounted by a swept blade strut that attached at top of model ahead of the inlet, or by a rear-entry sting that held the model at the location of the nacelle. The model had alternate parts for ±0.5° deflections of the flaps, ailerons, and stabilator, and ±1° deflections of the T-tail. Off-body static pressure measurements of the flow field below the model were made on a pressure rail which had 420 orifices along its tip. The model was positioned at various heights from the rail by vertical movement of the tunnel strut, and at various longitudinal stations relative to the rail by means of a linear actuator mounted between the wind tunnel strut and the balance. Spatial averaging of model pressure signatures acquired over a range of longitudinal positions reduced the effects of tunnel flow distortions and the interference of the rail flow field and shocks on the model pressure signatures. The test was run at approximate Mach numbers of 1.36, 1.4, and 1.47, and the model was set at various angles of attack and roll relative to the rail. Plots of the model signatures for representative variations of Mach number, model angles, control deflections, and height relative to the rail are provided throughout the report. Repeatability was generally very good and gave confidence in the quality of the measurements. The signatures measured at various heights from the rail provided insight into the aging of the model shocks as they propagated from 1.2 to 3 body lengths from the model. Off-track signatures up to 45° from centerline obtained by rolling the model gave indications of the shock flow fields across the width of the sonic boom carpet. The deflections of the various control surfaces allowed assessment of the boom sensitivity to the control surface movements.

---

[1] Aerospace Engineer, Experimental Aero-Physics Branch, Senior Member.
[2] Research Aerospace Engineer, Inlets and Nozzles Branch, Associate Fellow.
[3] Research Aerospace Engineer, Configuration Aerodynamics Branch, Senior Member.
[4] Research Aerospace Engineer, Configuration Aerodynamics Branch, Senior Member.
[5] Research Aerospace Engineer, Configuration Aerodynamics Branch, Senior Member.
[6] Research Aerospace Engineer, Configuration Aerodynamics Branch, Member.
[7] Research Aerospace Engineer, Configuration Aerodynamics Branch, Member.
[8] Research Aerospace Engineer, Configuration Aerodynamics Branch, Associate Fellow.
[9] Senior Aerodynamics Engineer, Flight Sciences.

Nomenclature

A	=	area
AMS	=	Angle Measurement System
B/LA	=	Balance/Linear Actuator adapter
BS/B	=	Blade Strut/Balance adapter
CAD	=	Computer Aided Design
CFD	=	Computational Fluid Dynamics
CoR	=	Center of rotation
$DewPt$	=	dew point, °F
DPC	=	corrected pressure signature magnitude, $\Delta P/P_U$ - $\Delta P/P_R$
FAA	=	Federal Aviation Administration
$Humidity$	=	freestream humidity in ppm by weight
$HumAvg$	=	average humidity over all data samples in a run
h, h_{Nose}	=	height of model nose above pressure rail, inches
$h/L, h_{Nose}/L$	=	height of model nose above pressure rail normalized by model length (18.80")
i	=	index of linear actuator ram positions (for uncertainty equations)
$ICAO$	=	International Civil Aviation Organization
j	=	index of two-second averages of data in data files (for uncertainty equations)
k	=	index for points in the X_4 vector (for uncertainty equations)
L	=	model length, 18.80"
LE	=	leading edge
$PLdB$	=	perceived level in decibels
P_{Rail}	=	static pressure at rail orifice, psf
P_∞	=	freestream tunnel static pressure, psi
q	=	dynamic pressure, psf
Re/L	=	Reynolds number per unit length
$SigSet$	=	Signature Set: set of runs over a range of linear actuator ram positions
$SweepInc$	=	X_{Ram} position increments in X sweep
$SweepRng$	=	Range of X_{Ram} positions in X sweep
TE	=	trailing edge
$TomoBOS$	=	tomographic background-oriented schlieren
V	=	velocity
X	=	longitudinal coordinate, along tunnel axis or rail edge
X/L	=	longitudinal coordinate normalized by model length
X_4	=	$X_{Orif} + X_{Ram}$ corrected for differences in model attitude and Mach number within a SigSet
X_{Orif}	=	longitudinal coordinate of rail orifice
X_{Ram}	=	Extension distance of linear actuator ram, from 0" to 24"
α	=	angle of attack, degrees
ϕ	=	angle of roll, degrees
ϕ_{m2r}	=	roll angle from model to rail (aka off-track angle for sonic boom propagation)
ϕ_{Model}, ϕ_{RM}	=	roll angle of model/roll mechanism relative to wind tunnel strut
$(\Delta P/P)_C$	=	corrected pressure signature magnitude, $\Delta P/P_U$ - $\Delta P/P_R$
$(\Delta P/P)_R$	=	uncorrected pressure signature magnitude for reference run, $[(P_{Rail} - P_\infty) / P_\infty]$
$(\Delta P/P)_U$	=	uncorrected pressure signature magnitude for data run, $[(P_{Rail} - P_\infty) / P_\infty]$

I. Introduction

THE Commercial Supersonics Technology (CST) Project[1] under NASA's Advanced Air Vehicles Program[2] (AAVP) has been focused on developing technologies for enabling designs of future commercial supersonic transport aircraft. Many different technology areas are being addressed, such as improving efficiency, reducing noise and emissions, but the greatest emphasis has been on reducing the sonic boom loudness.

NASA funded studies by Lockheed Martin[3,4] and Boeing[5,6] in 2009 to design low-boom commercial supersonic transport aircraft that would carry 50 to 75 passengers. The studies resulted in concepts that had estimated boom loudnesses with PLdB (perceived level in decibels) in the low 80s range. Small sonic boom models were made of these configurations and tested in supersonic wind tunnels at the NASA Ames and Glenn Research Centers.[7,8] Results

from the tests were compared to Computational Fluid Dynamics (CFD) predictions and served as validation test cases that have led to improvements in computational tool development for boom prediction.

In 2016, NASA initiated a project[9] aimed at designing and building a low-boom flight demonstrator aircraft with the primary purpose of achieving a flight-measured sonic boom loudness of 75 PLdB or less. Lockheed Martin was selected as the contractor to design and build the aircraft, designated as the X-59 by NASA. The acoustics of the aircraft will be validated through measurements of the boom pressure signatures by chase aircraft and on the ground, and responses from the public to what is hoped will be more of a benign sonic "thump" than a loud sonic boom will be gathered as the aircraft will be flown over various cities around the United States. The end goal of the project is to demonstrate that acceptably-low levels of boom loudness can be produced by an aircraft shaped for low-boom, and thus allow the regulators to open the door for commercial supersonic flight over land.

The flight test data from the X-59 will be compared to the CFD predictions of the near-, mid-, and far-field pressure distributions, and it was desired to obtain wind tunnel test data for additional comparisons. Thus a 1.62%-scale model of the X-59 configuration C612A was designed and fabricated by Tri Models, Inc., in 2020, and was run in the Glenn Research Center 8- by 6-Foot Supersonic Wind Tunnel in the fall of 2021.[10] The purpose of this paper is to present information about this test and provide a summary analysis of the data. The reader is referred to a NASA TM[11] which was recently published and provides more details about the test and a more comprehensive review of the data. A companion NASA TM[12] was also recently published and provides a comparison of CFD predictions and the wind tunnel data.

II. Test Objectives and Overview

The primary objective for the experiment was to acquire pressure signatures of the X-59 configuration for validation of computational models used in sonic boom prediction, and to be able to compare these signatures with the flight-test measurements. Secondary test objectives included acquisition of schlieren and tomographic background-oriented schlieren (TomoBOS) imaging to gain further insight into the flow field around the X-59 airframe and to provide validation images for CFD.

Data were measured in the test among variations in Mach number, near-field propagation distance (model height relative to a pressure rail), angles of attack and roll, and control surface deflections. The model was tested with two different mounting options: a 65°-swept blade strut that attached to the top of the model ahead of the engine inlet, and a rear sting that attached to the model at the location of the engine nacelle. The model had alternate parts for ±0.5° deflections of the flaps, ailerons, and stabilators, and ±1° deflections of the T-tail horizontal surface.

The primary data from the test were static pressures measured on a thin blade-type pressure rail that had a line of 420 orifices along its tip over a 66" length. To get better-quality data than just from single pressure signature measurements on the rail, a linear actuator was used to measure signatures at different longitudinal positions (typically 26) on the rail. These X sweeps of the model enabled spatial averaging of the signatures from the different positions, which greatly reduced the scatter of the data but did result in some rounding of the peaks in the signatures.

In addition to running the X-59 model, an axisymmetric calibration body, designated AS-2, was run to obtain simple pressure signatures for validation of the test techniques.

III.   Glenn 8- by 6-Foot Supersonic Wind Tunnel

The NASA Glenn Research Center 8- by 6-Foot Supersonic Wind Tunnel[13,14] (8x6) is part of a facility which includes a 9- by 15-Foot Low-Speed Wind Tunnel (9x15) test section on the opposite leg. Tests are run in one test section or the other, but not in both sections at the same time. The facility is a continuous-flow circuit, powered by three motors of 29,000 hp each, driving a seven-stage axial flow compressor. The 8x6 test section flow speed is 8' tall by 6' wide by 23.5' long. The tunnel has a wide Mach number range from 0.25 to 2.0, and the subject test was run at approximate Mach numbers of 1.36, 1.4, and 1.47.

The tunnel air is dried during operations by passing it over eight layers of large desiccant beds in the air dryer (just upstream of the compressor). The dryer beds are "reactivated"—removing the moisture by heating—with the compressor not running, during an off-shift each day in preparation for the next shift's running. The maximum acceptable dew point during wind-on operations is determined for each test, and operations are typically terminated during a running shift if the dew point exceeds this level.

The 8x6/9x15 wind tunnel complex is an atmospheric facility; there are no provisions for controlling the pressure in the tunnel aside from the normal pressure variation with flow speed. In addition, there is no after-cooler or radiator section between the compressor and the 8x6 test section, so the compression of the air causes the total temperature of

the air in the test section to be at or above 140° F at low supersonic Mach numbers, and higher temperatures at higher Mach numbers.

IV. Wind Tunnel Models and Support Components

Descriptions and geometry information for the two wind tunnel models and their support components are provided in this section.

A. AS-2 Model

The AS-2 model[6] (Figure 2 and Figure 2) was one of several sonic boom models designed by The Boeing Company in 2010 under contract to NASA in an experimental systems validation study for supersonic transport aircraft. The AS-2 was designed to be used as an axisymmetric calibration body in sonic boom wind tunnel testing. Its geometry consists of an ogive nose, a constant cylindrical section, a conical section to match the diameter of the support hardware behind the model, and a male taper adapter to fit within the support piece. In the case of this test, the support piece was a balance adapter that fit around the balance that was used for force measurements. The simple external shape of the AS-2 model was designed to create a simple, predictable pressure signature that could be used to give an indication of the quality of the wind tunnel flow and the measurement of the off-body pressures along the pressure rail. It has been used in previous model tests in the 8x6 tunnel and in the Unitary Plan Wind Tunnels at NASA Ames Research Center.
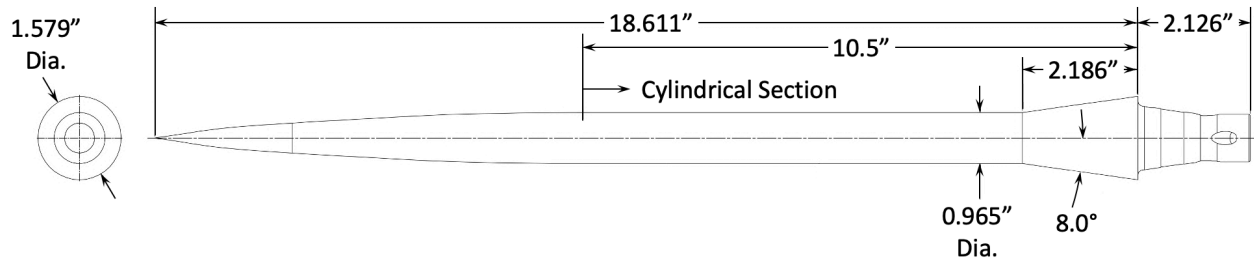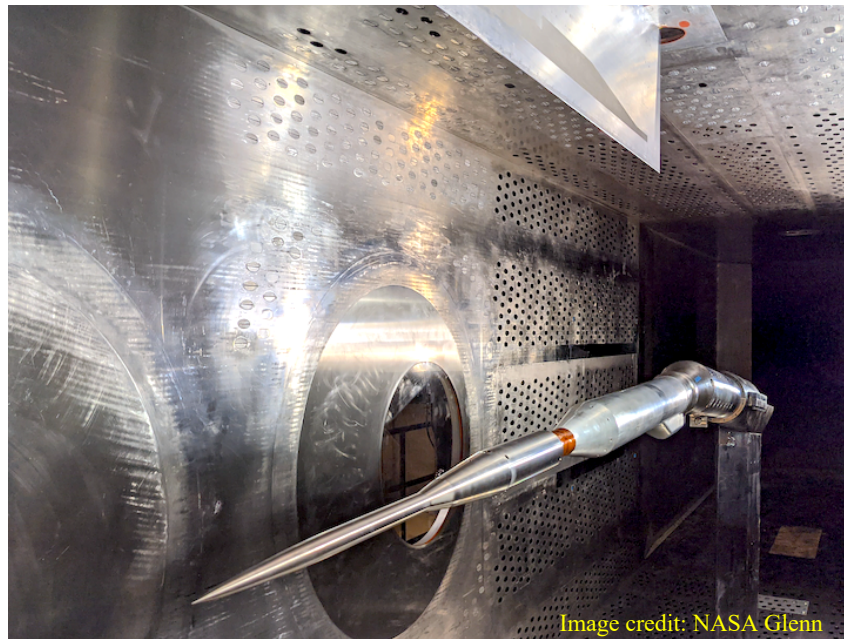

Figure 1   Geometry of AS-2 model

Image credit: NASA Glenn

Figure 2 Photograph of AS-2 model installed in 8x6 wind tunnel showing rail on ceiling

4

B. X-59 Aircraft and Sonic Boom Model

The X-59 flight demonstrator aircraft[16] (Figure 3) has been designed by Lockheed Martin under contract with NASA to have a quiet sonic boom from its cruise flight condition of Mach 1.4 at 55,000 ft altitude. The boom loudness is expected to be about 75 PLdB at ground level.
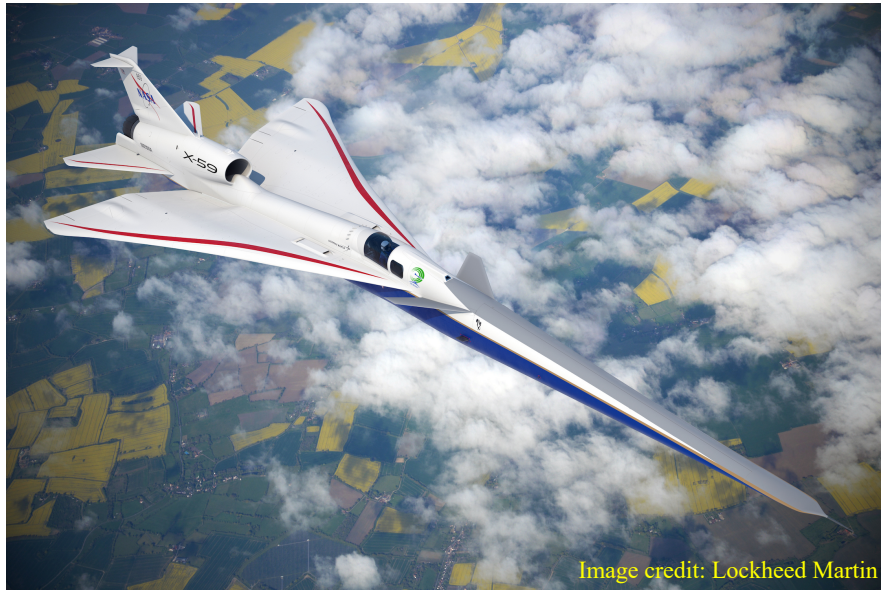

Image credit: Lockheed Martin

Figure 3 X-59 flight demonstrator aircraft

An 18.80-inch long, 1.6212%-scale model of the C612A version of the X-59 aircraft was designed and fabricated by Tri Models, Inc. The model features interchangeable wing aft sections with various flap and aileron deflections, a horizontal stabilator, and T-tail that can be set at various deflection angles, and two means of mounting the model to its support structure—a swept blade strut and a rear-entry sting. Views of the model and its deflectable control surfaces are provided in Figure 4 and Figure 5. All the control deflections are positive trailing-edge down, and all deflections (including the ailerons) are symmetric left/right. This symmetry is for sonic boom tailoring; rolling moment effects on boom were not an objective of this test.
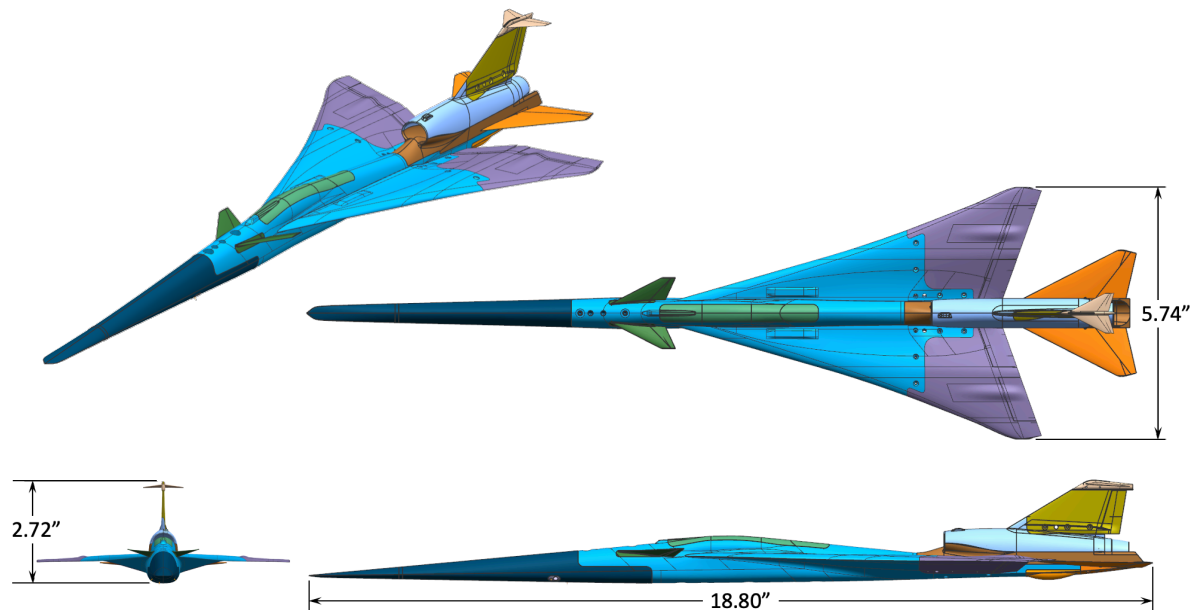

Figure 4 Four-view of X-59 1.62%-scale model

	Flaps	Ailerons
Wing1	-2.4°	1.1°
Wing2	-2.4°	1.6°
Wing3	-2.4°	0.6°
Wing4	-2.9°	1.1°
Wing5	-1.9°	1.1°

T-tail
2.7°
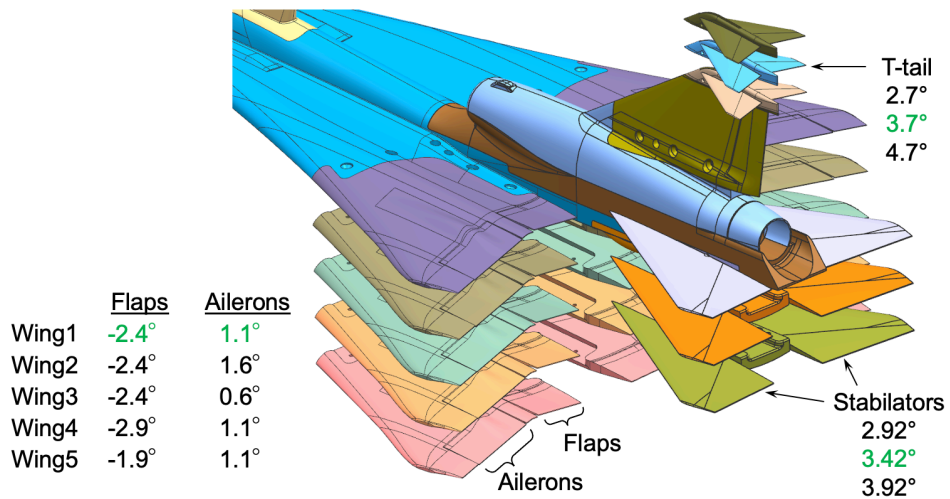3.7°
4.7°

Stabilators
2.92°
3.42°
3.92°

Figure 5 X-59 model control surface deflection options (+ TE down), baseline angles for cruise flight in green

Photographs of the X-59 model and the pressure rail mounted in the ceiling of the Glenn 8x6 are shown in Figure 6. In Figure 6(a), the model is inverted as in the running orientation so that the shocks from the bottom of the model would be directed to the rail.

Image credits: NASA Glenn

(a) View looking aft   **(b) View looking forward**

Figure 6   Views of X-59 model mounted on blade strut in wind tunnel with pressure rail mounted in the ceiling

C. X-59 Model Supports

The model was attached to the wind tunnel strut by various pieces of support hardware. This hardware, from the strut up to the force balance, consisted of a stub sting (fixed adapter), Ames Small Model Roll Mechanism (SMRM), linear actuator, balance / linear actuator (B/LA) adapter, and Langley 2.0"-diameter 750 balance. For mounting the model on the blade strut, a blade strut / balance (BS/B) adapter was used, and for mounting the model on the sting, the sting had its own integral balance adapter. CAD views of these adapters and parts forward of the linear actuator are shown in Figure 7, with the upper view showing the model mounted on the blade strut and the lower view showing the model mounted on the sting. The balance was used primarily for measuring the normal force of the assembly mounted to it so that the right deflection constants could be applied in setting the model angle of attack for the models. The other forces and moments from the balance (drag, side force, and the three moments) were not relevant to this test and were thus ignored.

Both the blade strut and the sting were designed to hold the model at 2.1° angle of attack (the cruise angle for the X-59 airplane flying at Mach 1.4) when the linear actuator and balance are level. This allows for the model to stay at the same vertical distance from the rail when it is moved forward in an X sweep, since the linear actuator is level with the rear parts of the blade strut and sting.
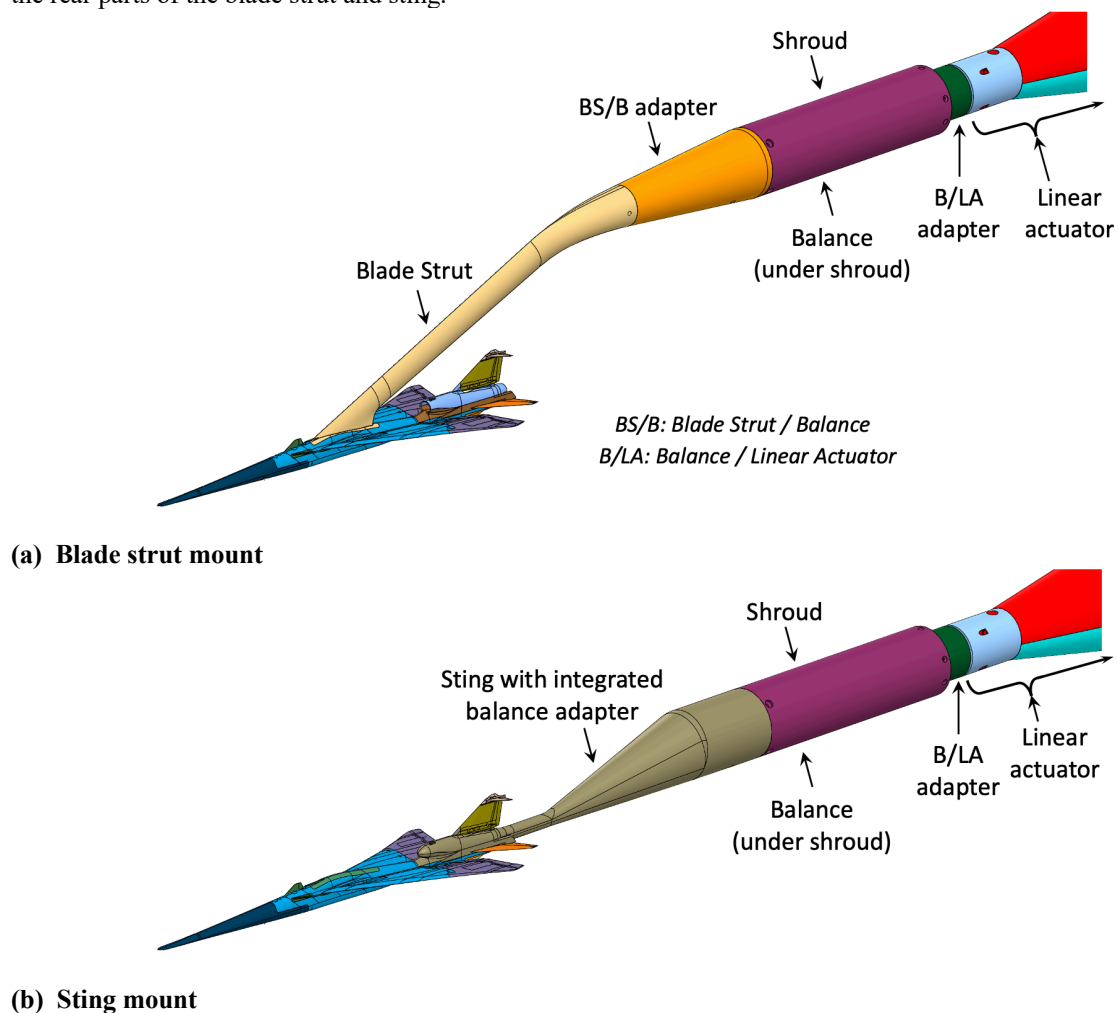

(a) Blade strut mount

(b) Sting mount

Figure 7 Support options for X-59 sonic boom model

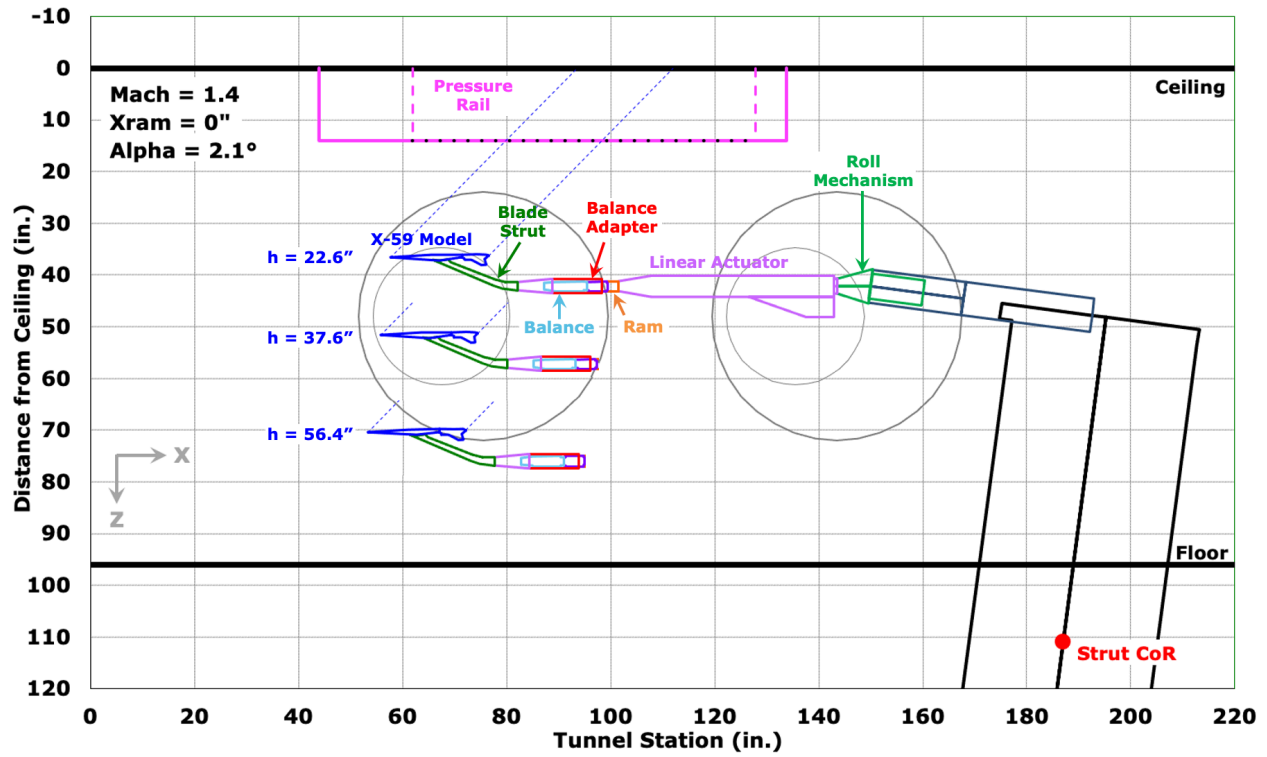### D. Wind Tunnel Layout Diagrams

Layout diagrams of the model at various heights of the nose below the rail are given in Figure 8. Subfigure (a) shows the model mounted on the blade strut at the three different heights run in this test. These same heights were also run for the sting-mounted configuration, which were enabled by positioning the tunnel strut higher by the difference (4.64") between the vertical offset distances for the blade strut (5.52") and the sting (0.88"). In most of the data plots presented in Section VI, the model height will be specified in terms of h/L, where $L = 18.80$", the model body length. The model heights shown in Figure 8(a) of 22.6", 37.6", and 56.4" correspond to h/L values of 1.2, 2.0, and 3.0, respectively. The lowest and highest heights were near the limits of the vertical range of the tunnel strut movement. The roll mechanism is set at 0° roll in this subfigure so that the bottom of the model faces the rail.

Subfigure (b) shows the model in position for a reference run. The use of a reference run to correct the model pressure signatures will be discussed in Section VI. The linear actuator ram (the short segment shown in orange between the linear actuator housing and the balance adapter) is fully retracted in these views, and the roll mechanism is set at 180° roll to position the model nose shock as far aft on the rail as possible.

The 90"-long pressure rail mounted on the ceiling of the test section has a 66"-long instrumented section consisting of 420 static-pressure orifices, which are denoted by the black dots along the tip between the vertical dashed lines on the rail (from tunnel station 61.9" to 127.9"). The shocks coming from the nose and rear of the model are drawn at the Mach line angle—44.4° from vertical — for Mach 1.4. No attempt was made to account for aging of the shocks nor for changes in reflections off the ceiling due to tunnel boundary layer in this layout. Rather, the shock lines were used to provide guidance for setting the model height and linear actuator extension range for each signature X sweep more than for trying to predict exactly where the model shocks would intersect the rail.

The SMRM that was used in this test has a fixed 7.5° offset which made it necessary to pitch the tunnel strut by the opposite of this amount to set the model at its nominal angle of attack of 2.1° (corresponding to the balance and linear actuator being level in the tunnel, except when other model pitch angles were desired). Note that since the model blade strut and sting locate the centerline of the model a short vertical distance from the rotation axis of the roll mechanism (along the centerline of the balance and linear actuator), the roll angle of the SMRM is not the same as the roll angle from the model to the rail. Reference 11 provides a graphic illustrating the difference between these two angles. In the pressure signature plots later in this paper, the model roll angle is referred to as ϕ_{m2r}, model-to-rail roll angle.

The wind tunnel strut raises and lowers through the tunnel floor to change the height of the model. For changing pitch angle, the strut pivots about a center of rotation that is 15" below the floor, so for an increase in model angle of attack, the model moves forward in the tunnel slightly (~1" forward for a 1° angle increase, with model 22.6" below the rail).

(a) X-59 model at heights for data runs, $\alpha = 2.1°$, $\phi = 0°$
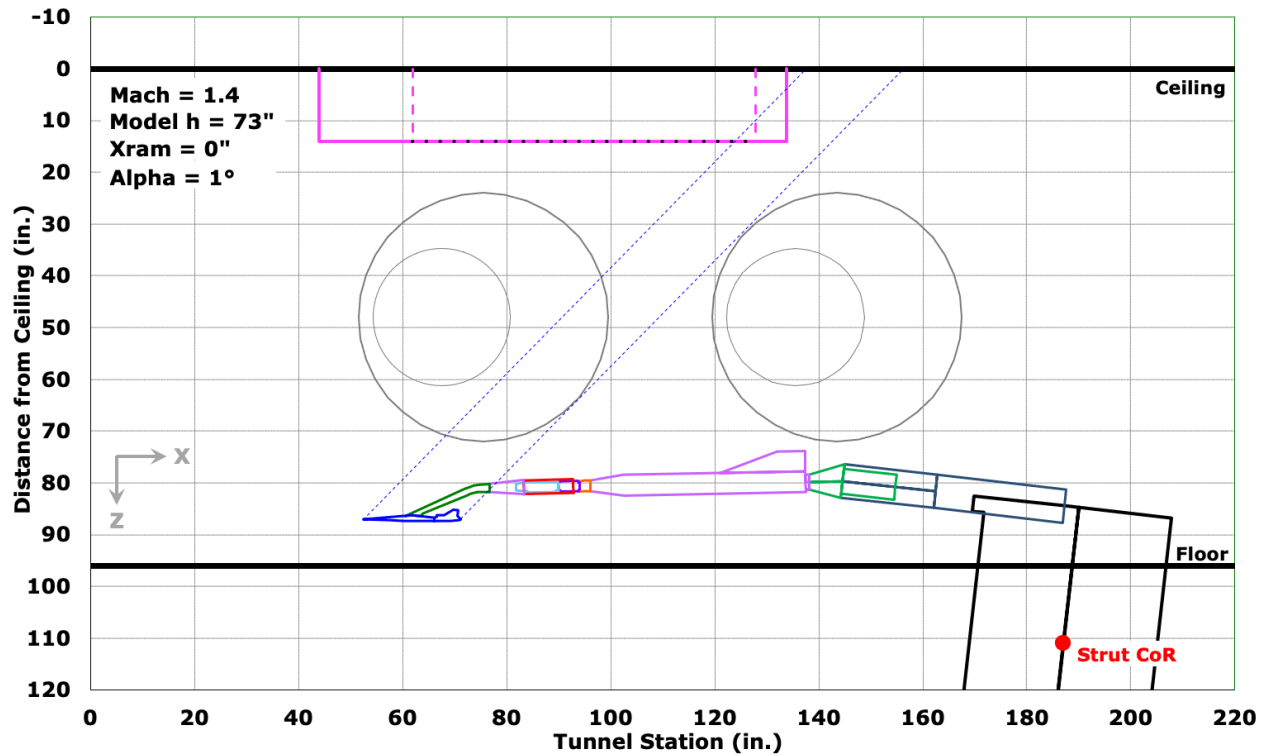
(b) X-59 model at height for reference runs, $\alpha = 1°$, $\phi = 180°$

Figure 8 Layout diagrams of model in tunnel
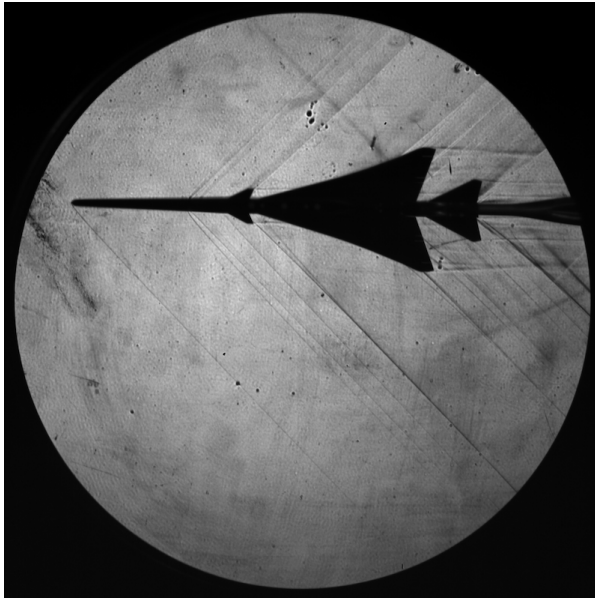
V. Schlieren Imaging

Schlieren images of the model with the sting mount were acquired using an Imperx Cheetah 16MP camera. High-resolution images of the flow field surrounding the model were acquired in sets of 100 and were averaged to remove background flow. A few of the schlieren images obtained during the test are presented in Figure 9. The model was set at roll angles (not model-to-rail angles) of 0°, 45°, and 90° to show the differences in shock structure from the different views around the model. The first image (a) has been cleaned up to remove artifacts in the image that do not represent the flow features from the model, but the latter two images have not been cleaned up. They contain shock or expansion waves that cross the model shocks and are from unknown sources away from the model, and there are localized darkened areas in the images that are likely from unknown defects in the optical path.
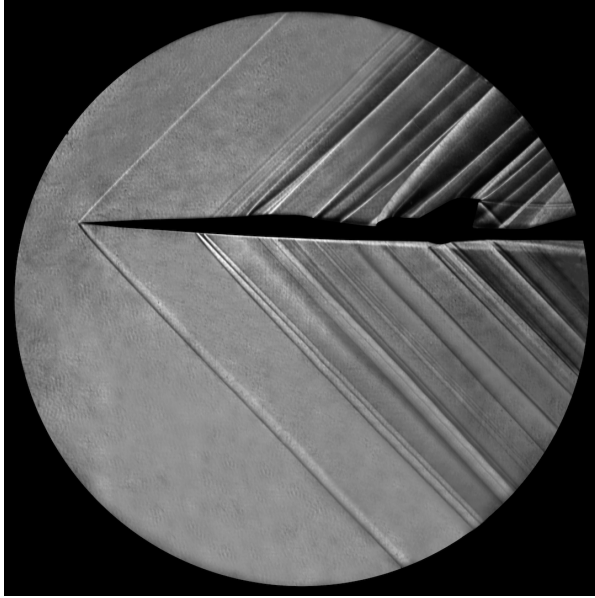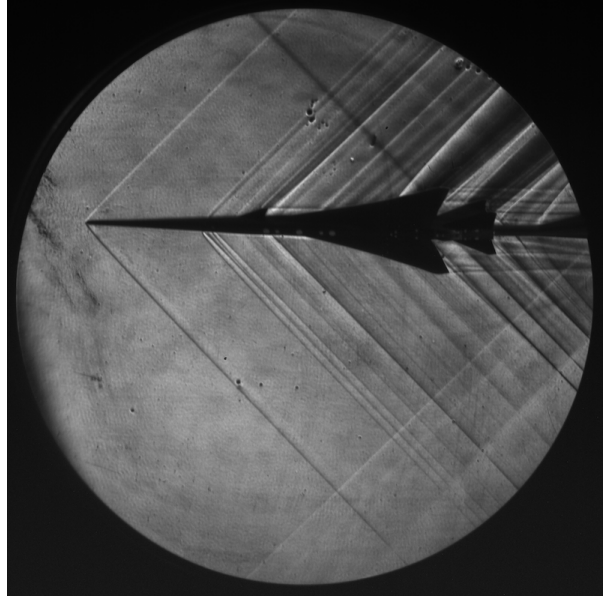
(a) $\phi_{RM} = 0°$ **(b) $\phi_{RM} = 45°$**

(c) $\phi_{RM} = 90°$

Figure 9 Schlieren images of X-59 model with sting, Mach 1.4, $\alpha = 2.1°$

VI.   Results and Discussion

The test techniques, data reduction methods, uncertainty estimation, and analysis of the effects of model and test condition variations on the measured pressure signatures are presented in this section. In all the data plots that follow, the model angles of attack and roll, and all control surface deflections, are at their nominal angles unless otherwise stated in the plot titles or legends. These nominal angles are:

- angle of attack = 2.1°
- angle of roll = 0°
- flaps = -2.4°
- ailerons = 1.1°
- stabilators = 3.42°
- T-tail = 3.7°

A.   Data Acquisition

Data were acquired for this test with the facility's Cobra data-acquisition system. The system sampled all the data channels at 12.5 Hz, and the following sampling durations were set for the different types of runs:

- 5 seconds for pitch runs
- 60 seconds for reference runs
- Pressure signature data runs: initially 60 seconds, then down to 30 seconds and ultimately down to 15 seconds a few days into the test after observing that the data quality did not significantly change with the shorter durations

Pitch runs for the purpose of flow angularity measurements consisted of progressive series of model angles of attack with all other model and tunnel conditions held constant. Reference and data runs referred to data taken for empty-tunnel and model pressure signatures on the rail, respectively, and consisted of data sampled over a specified duration with all tunnel and model conditions held constant. The difference between reference and data runs is that the former were acquired with the model as far aft and away from the rail as possible so that the pressure distribution on the rail would represent the variation of the tunnel flow without the influence of the model. Ideally, none of the model shocks would be on the rail for the reference runs, but in this test, the model nose shock passed over the last few inches of rail orifices in the reference runs, as shown in Figure 8(b). For data runs, the model was moved closer to the rail so that the shocks from the entire length of the model fell on the rail. After sampling the data for the desired duration, the model was moved forward slightly (usually 0.32", approximately equivalent to twice the orifice spacing on the rail) by the linear actuator, the run number was incremented, and data were taken for the same duration. This process continued until the desired length of the X sweep was completed, and the entire sweep, which typically consisted of 26 runs, was labeled as a Signature Set, or SigSet for short.

Reference runs were acquired frequently in the test so that the data runs which used them would be fairly close to them in time, thus minimizing any adverse effects of changes in the tunnel flow or ESP scanner properties. The data acquisition system was set up so that a data run would use the most recent reference run by default, but if the test customer determined that an ending reference run after a set of data runs would provide a better correction for the data runs, this was easily accommodated in post-processing. The process for correcting data runs with reference runs is described in detail in reference 11.

Review of the measured pressure signature plots in real time during the test gave insight into the data quality and whether there were any problems with the data. Bad rail pressure readings were usually obvious with consistently low or high values relative to nearby pressures, and the rail pressure parameters in the data for the bad ports were flagged with the value of 9999.

## B.   Pressure Signature Measurements and Spatial Averaging

The non-uniform flow field of the wind tunnel causes pressure signatures on the rail to be different for different model positions in the test section. Spatial averaging is used to produce a model pressure signature with reduced effects from the tunnel flow field spatial distortions. A set of 26 individual signatures and their spatial average from an X sweep are shown in Figure 10 and Figure 11 (all but the first and last runs are removed from the legend for brevity, but the numbers for all the runs are provided in the lower plots of each figure). In the first figure, the signatures are plotted by the rail orifice locations, and the forward movement of the linear actuator ram in 25 steps of 0.32" (spacing of about 2 rail orifices) from 16" to 24" extension is reflected by the shifting of the model signatures to the

left. In the second figure, the signatures are aligned by adding the X_{Ram} positions to the orifice locations for each run so that an average of all the pressures can be taken, which makes up one average pressure signature for a SigSet.

Note that in the first figure, there is a steep rise in pressure just beyond $X = 99$" for the first run and the average run, and the location for this pressure rise moves forward with the ram movement. This rise occurs just beyond $X = 115$ for *all* the runs in the second figure because they are aligned with X_{Ram} having been added to X_{Orif}. These pressure rises are from the shock from the rear of the model blade strut where it makes a transition from the biconvex blade shape to a circular cross section for mating with the balance adapter. The model shocks can be considered terminated just prior to these pressure rises.

The upper plots in each of Figure 10 and Figure 11 are *overlay* plots, where the signatures are plotted with their unmodified pressure values. The lower parts of the figures contain *waterfall* plots, for which the pressure values are plotted with a progressive -0.005 $\Delta P/P$ offset for each successive signature. The overlay plots give an indication of the repeatability of the signatures, while the changes from one signature to the next can be observed in the waterfall plots.

Note in the overlay plot of Figure 11 that the repeatability is very good from the nose shock back to $X_{Orif} + X_{Ram}$ around 100", but the repeatability is not as good in the middle part of the signature and only slightly better toward the rear of the signature until about 110" where the scatter reduces. The reason for this variation in scatter over the length of the signature is not known.
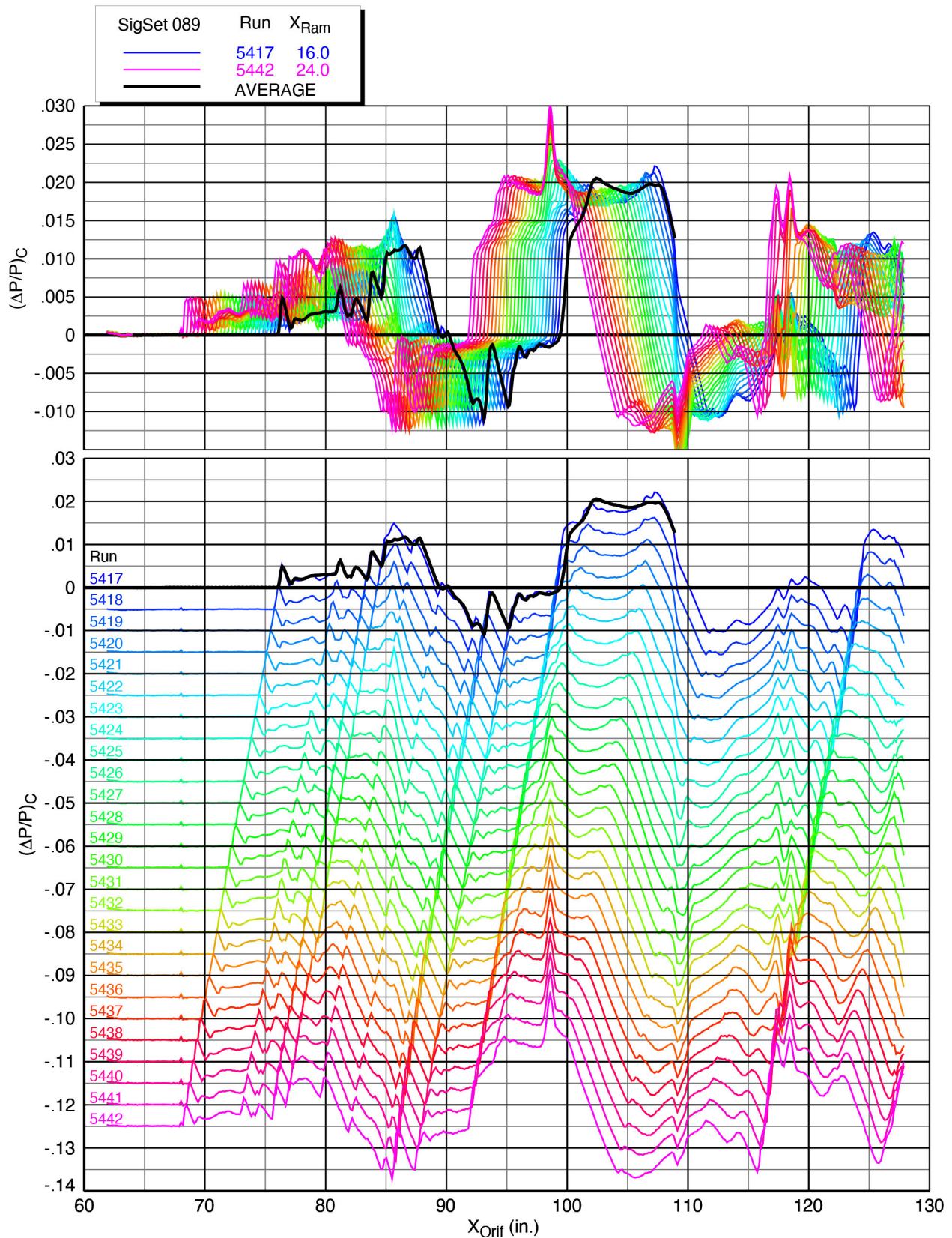
Figure 10 Unaligned pressure signatures for SigSet 89 in overlay and waterfall plots
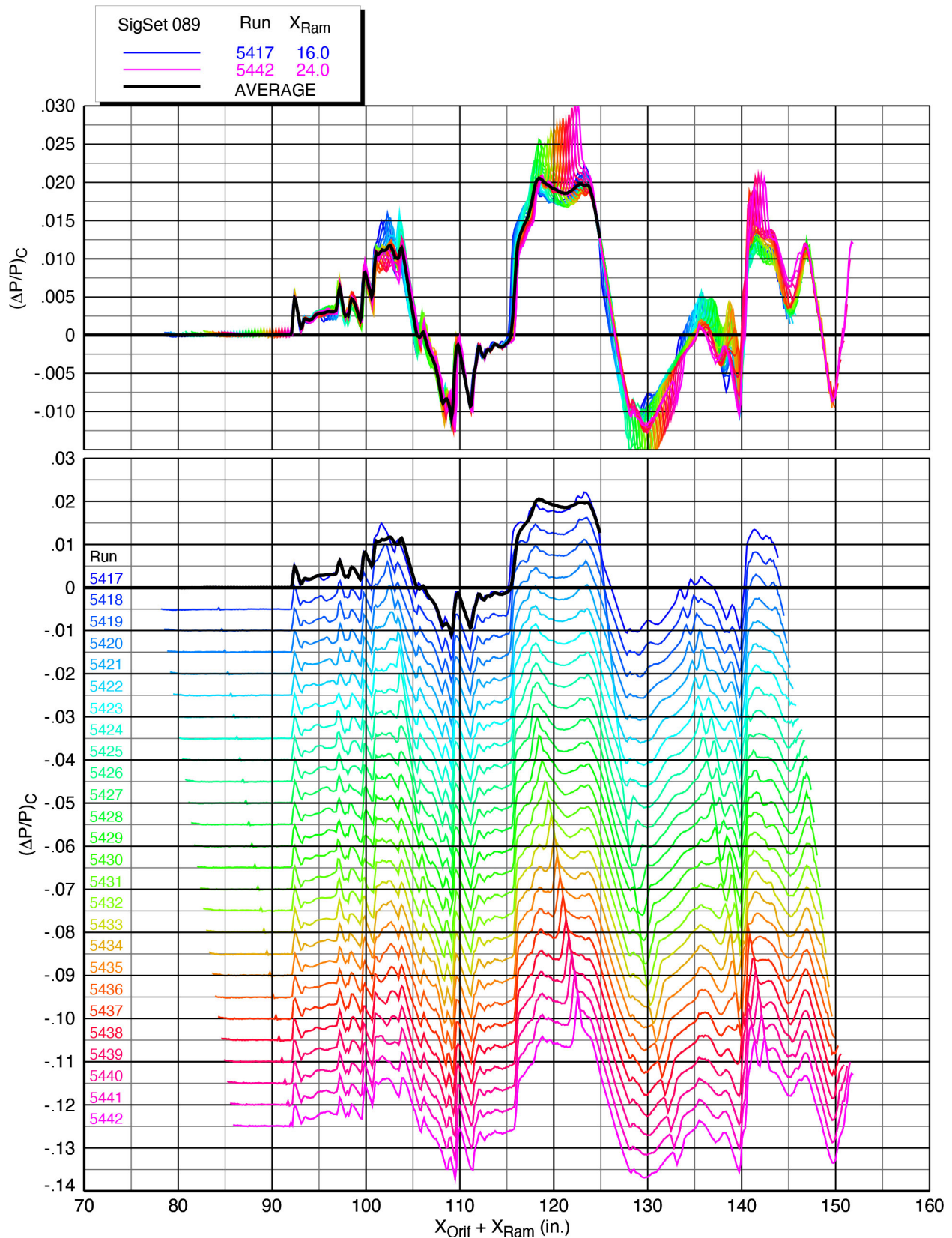**X-59 model (blade strut), Mach 1.4, $h/L = 2$, $\alpha = 2.1°$, $\phi_{m2r} = 0°$**

13

Figure 11 Aligned pressure signatures for SigSet 89 in overlay and waterfall plots
X-59 model (blade strut), Mach 1.4, $h/L = 2$, $\alpha = 2.1°$, $\phi_{m2r} = 0°$

C. Repeatability and Uncertainty

A plot of repeatability among four SigSets of X-59 model signatures at Mach 1.4 is presented in Figure 12. The agreement is excellent over almost the entire length of the signatures, though there are some very small differences toward the rear. Note the large span of humidity among these four SigSets—from 119 to 867 ppm. The good agreement among the curves, with no discernable trends of pressure increases or decreases with humidity, indicates that humidity did not have any significant effect on the data (as supported by many other figures in Reference 11).
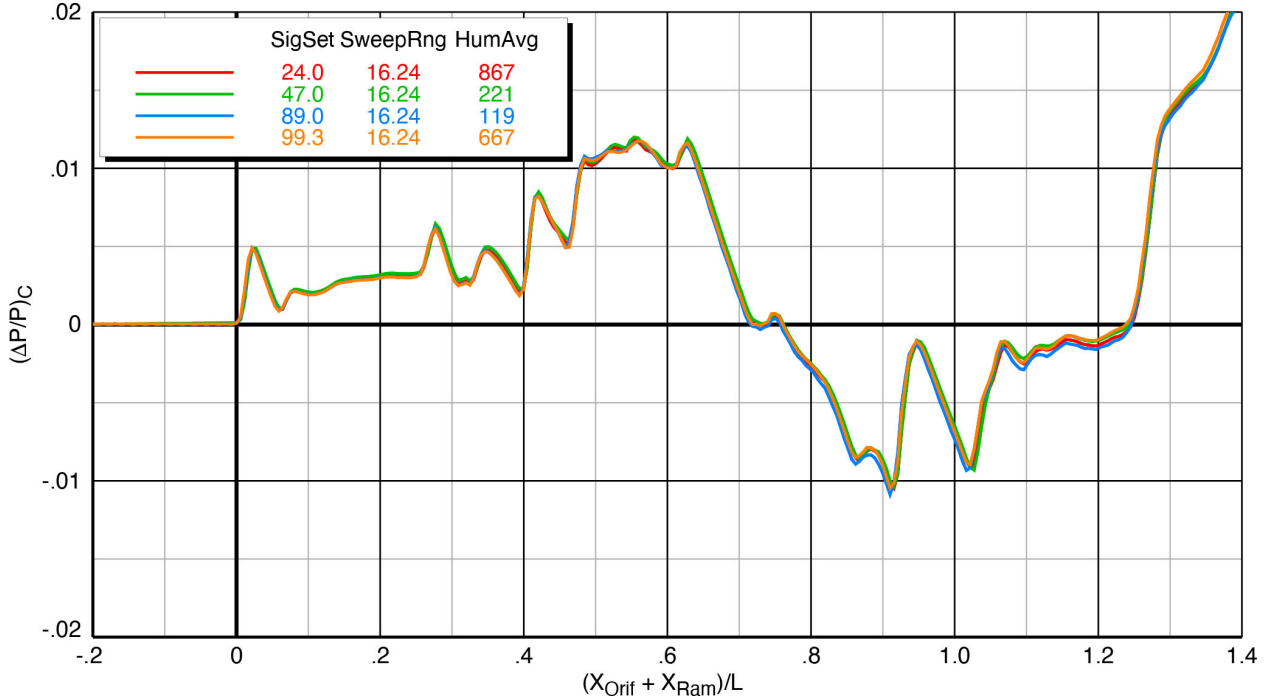
Figure 12 Repeatability of X-59 model (blade strut) signatures, Mach 1.4, $h/L = 2$, $\alpha = 2.1°$, $\phi_{m2r} = 0°$

An uncertainty analysis was conducted for the data in this test, in which the uncertainty can be used to represent the 95% confidence bounds that a repeated averaged dataset, $\overline{DPC}$, will fall in the range of $\overline{DPC} \pm 2\sigma_{\overline{DPC}}$. It should be noted that using 2σ to define the 95% coverage implies a normal distribution; however, it is best to not assume a distribution given the low sample sizes for the experimental data. The grand mean signature from SigSet 89 is plotted with the $\pm 2\sigma$ uncertainty bounds in Figure 13.
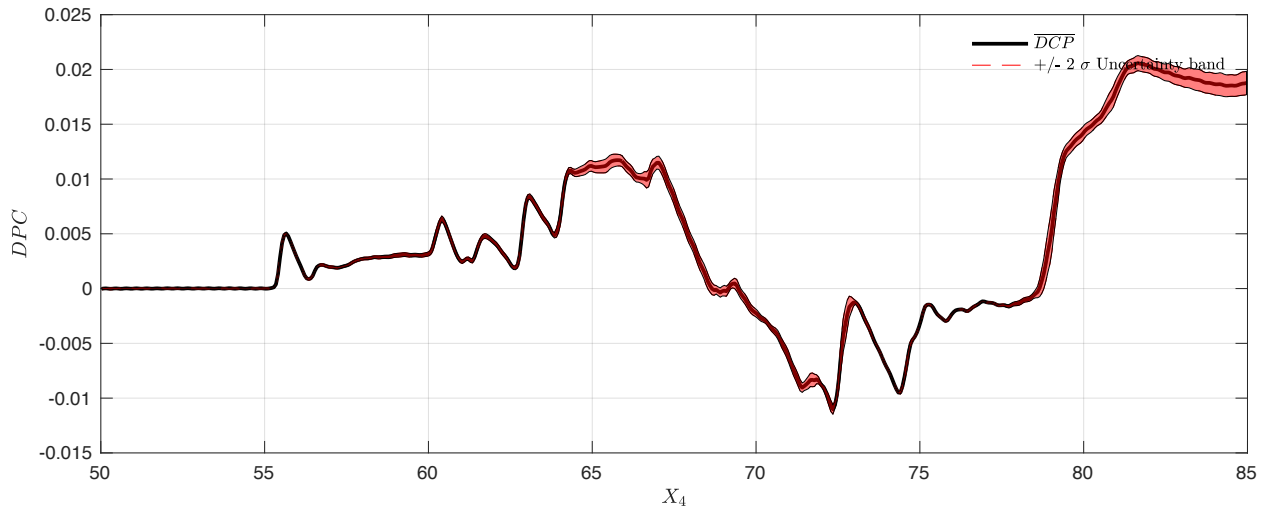

Figure 13 Grand mean signature with uncertainty bounds at ±2σ for SigSet 89

15

D. Effect of Control Surface Deflections

Plots showing the effects of deflecting the stabilator, T-tail, flaps, and ailerons on the X-59 pressure signatures are provided in this section. Single plots are shown for each control surface effect at the baseline conditions of Mach 1.4, $h/L = 1.2$, $\alpha = 2.1°$, $\phi_{m2r} = 0°$, and plots at other tunnel and model conditions are provided in reference 11.

1. Effect of Stabilator Deflections

Figure 14 presents averaged signatures for the X-59 blade strut configuration with stabilator angles of 2.92°, 3.42°, and 3.92°. With the stabilator being at the rear of the vehicle, the changes in the pressure signatures are expected to be seen near the end of the signatures. In the plot below, the changes are observed in the region of X/L (short for $(X_{Orif} + X_{Ram})/L$) = 0.9 to 1.1, and the portion of the signature ahead of this is not impacted. As the stabilator is deflected and producing more or less lift than at the nominal angle of 3.42°, the change in shock strength for that portion of the signature is evident in all of the plot.
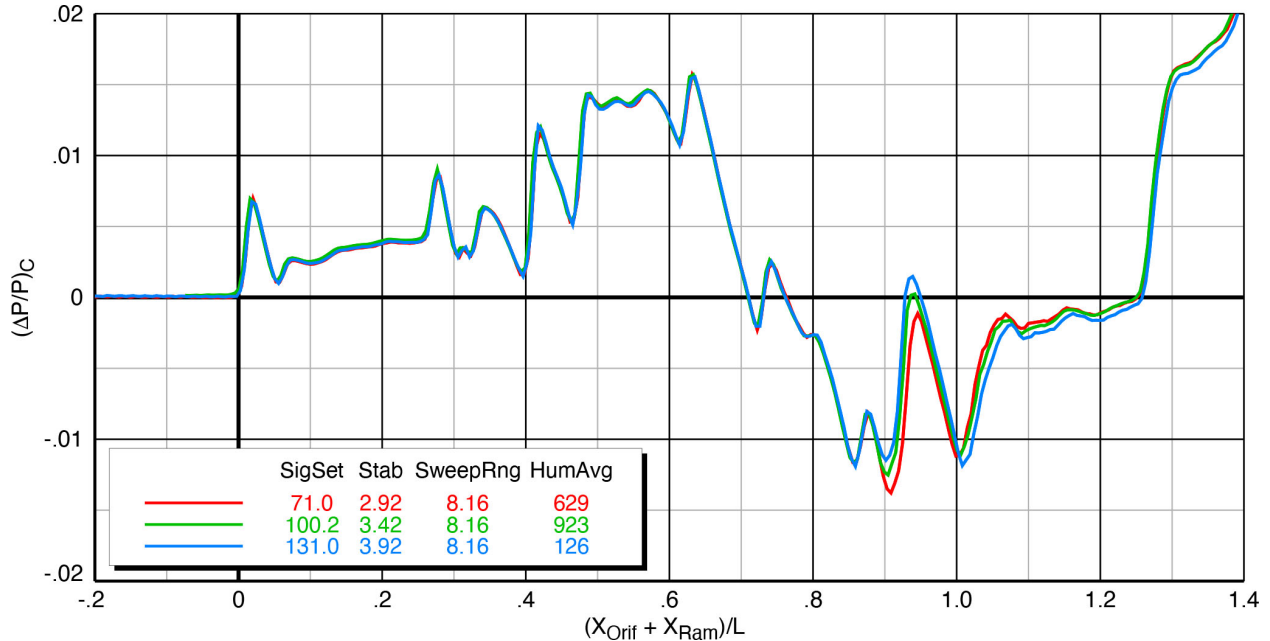

Figure 14 Effect of stabilator deflections on X-59 model (blade strut) spatially-averaged pressure signatures, Mach 1.4, $h/L = 1.2$, $\alpha = 2.1°$, $\phi_{m2r} = 0°$

2. Effect of T-tail Deflections

Signatures with T-tail deflection angles of 2.7°, 3.7°, 4.7° are presented in Figure 15. The T-tail is directly above the stabilator on the X-59, but its influence on the pressure signatures is aft of that of the stabilator because the shocks propagate downward from the vehicle roughly along the Mach line angle (~44° for Mach 1.4). Thus, the increments in the shock locations from the T-tail should be just aft of the stabilator shocks, and they do appear in the three plots below in the region of X/L = 1.02 to 1.05. The portions of the signatures in this region show the normal progression of the shocks moving forward with increasing T-tail deflection, though the increments are very small. The T-tail was added to the vehicle to aid in tailoring the merging of the shocks in the aft part of the signature and allow some variation of the sonic boom loudness.
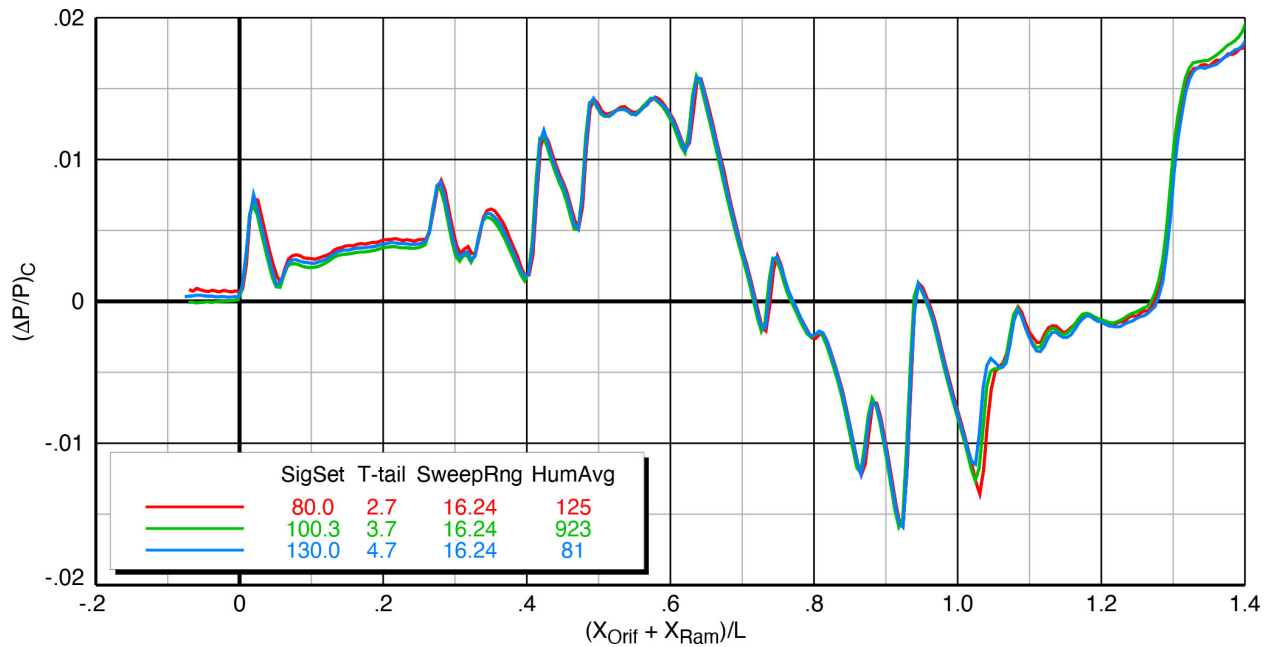
Figure 15 Effect of T-tail deflections on X-59 model (blade strut) spatially-averaged pressure signatures,
Mach 1.4, $h/L = 1.2$, $\alpha = 2.1°$, $\phi_{m2r} = 0°$

3. *Effect of Flap Deflections*

The effects of deflecting the flaps to angles of -2.9°, -2.4°, and -1.9° on the model signatures are presented in Figure 16 for the X-59 model mounted on the sting. Increments in the signatures from the flap deflections are apparent in the plot in the *X/L* range of approximately 0.7 to 1.0, partially overlapping the range in which the stabilator increments were seen. The primary effect of the flap deflection is in the *X/L* range of 0.7 to 0.8, and the differences among the curves downstream of this are a result of the changes in flap downwash on the stabilators with deflection angle.
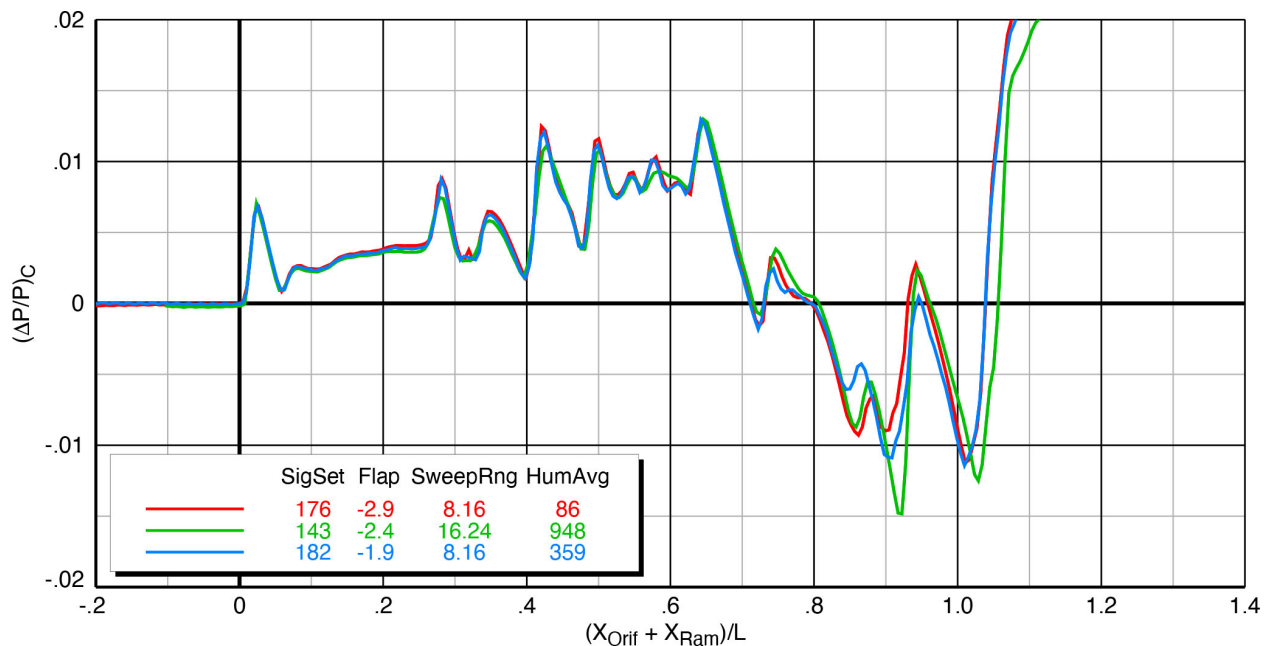

Figure 16 Effect of flap deflections on X-59 model (sting) spatially-averaged pressure signatures,
Mach 1.4, $h/L = 1.2$, $\alpha = 2.1°$, $\phi_{m2r} = 0°$

4. Effect of Aileron Deflections

The aileron deflection effects are presented in Figure 17 for aileron angles of 0.6°, 1.1°, and 1.6°. The increments in the signatures from the aileron deflections are in the same approximate *X/L* range identified for the flap deflections. Recall that the aileron deflections are symmetric on both sides of the wing, as opposed to one up and one down for roll control.

The effects of deflecting the ailerons on both model configurations are observed in the same region of the plots as for the flap deflections: from approximately *X/L* = 0.7 to 1.0. The changes in pressure values with deflection angles are fairly consistent over this region.
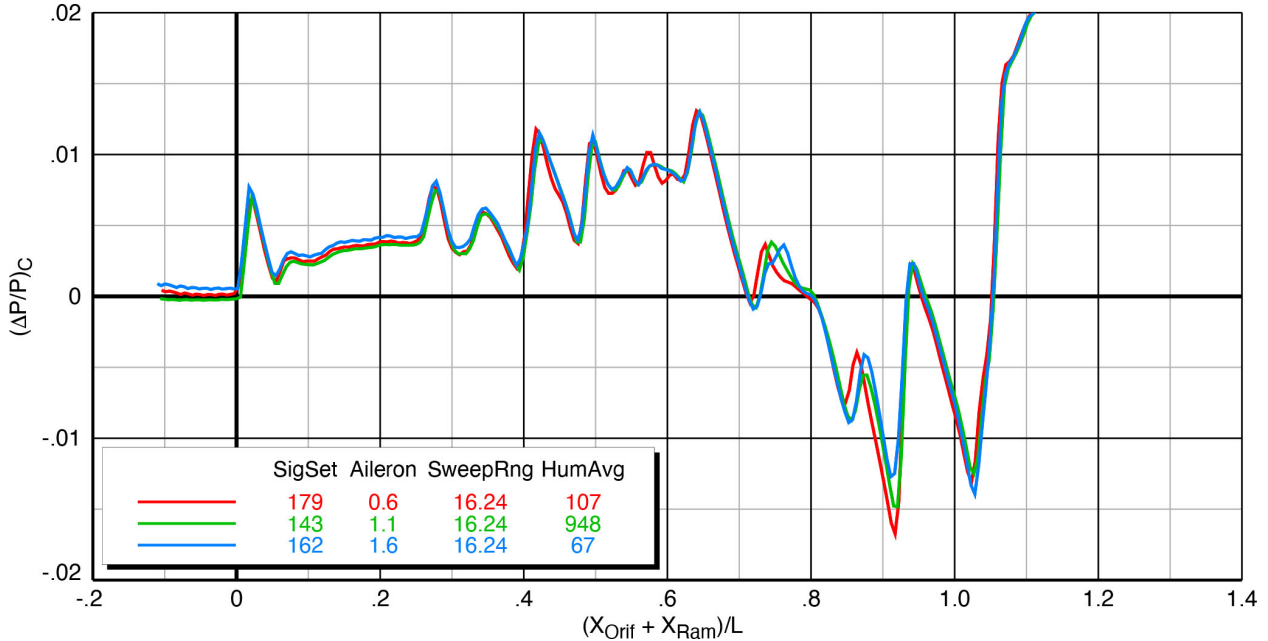

SigSet	Aileron	SweepRng	HumAvg
179	0.6	16.24	107
143	1.1	16.24	948
162	1.6	16.24	67

Figure 17 Effect of aileron deflections on X-59 model (sting) spatially-averaged pressure signatures, Mach 1.4, *h/L* = 1.2, α = 2.1°, ϕ_{m2r} = 0°

E. Effect of Angle of Attack

Figure 18 shows the effects of angle of attack on the model signatures. The plot shows that changes in the model angle of attack from 1.8° to 2.4° raise the overall pressure levels in the middle and aft portions of the signatures, but not in the forward part of the signatures up to about 0.3 *X/L*. The X-59's long nose has a mostly-rounded shape and is not intended to be a lifting surface, so it is not surprising that this portion of the signature does not show much sensitivity to angle of attack.. The lifting surfaces aft of this point show fairly consistent trends of higher pressure levels with angle of attack, but the individual shocks do not show significant strength increases, though they do move forward somewhat with increasing model angle.
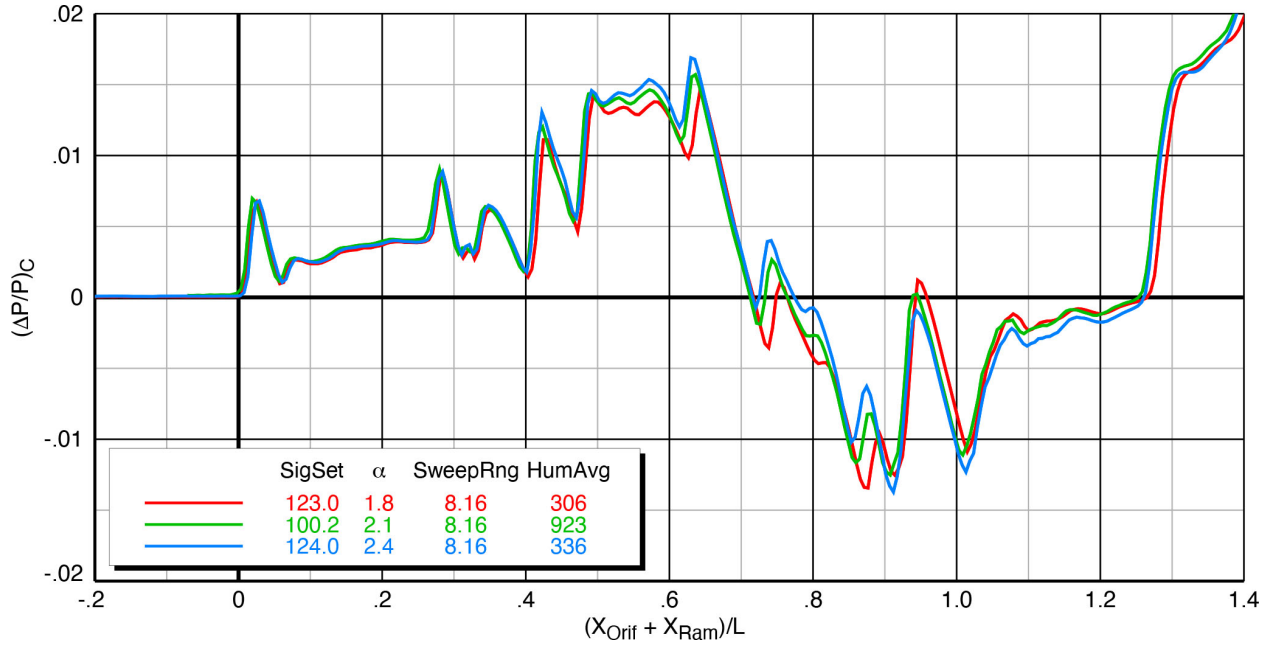
18

Figure 18 Effect of angle of attack on X-59 model (blade strut) spatially-averaged pressure signatures, Mach 1.4, $h/L = 1.2$, $\phi_{m2r} = 0°$

F. Effect of Height

Signatures measured at three different model heights relative to the rail are presented in Figure 19. Changing the model height relative to the pressure rail has a very large effect on the signatures as evidenced in this plot. Increasing the height shows the aging of the signatures in terms of decreasing overall pressure levels and shock strengths. The locations of the shock waves stay about the same at the different heights in the plots at all three Mach numbers and both model-mounting configurations.
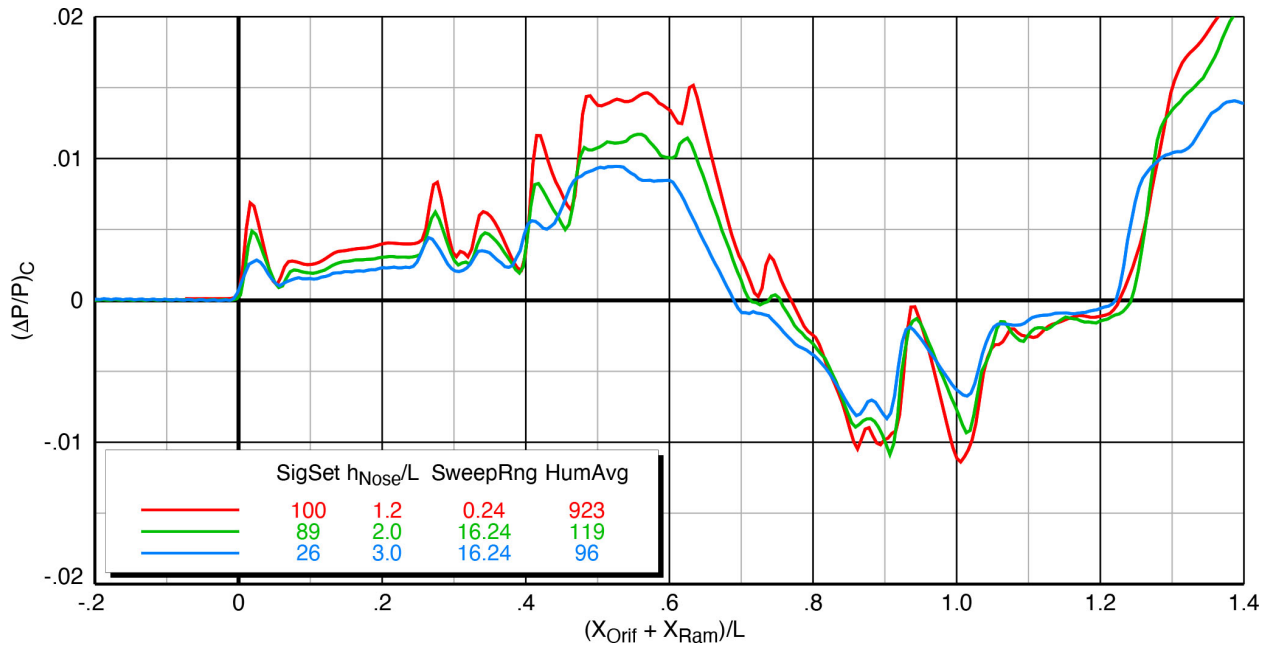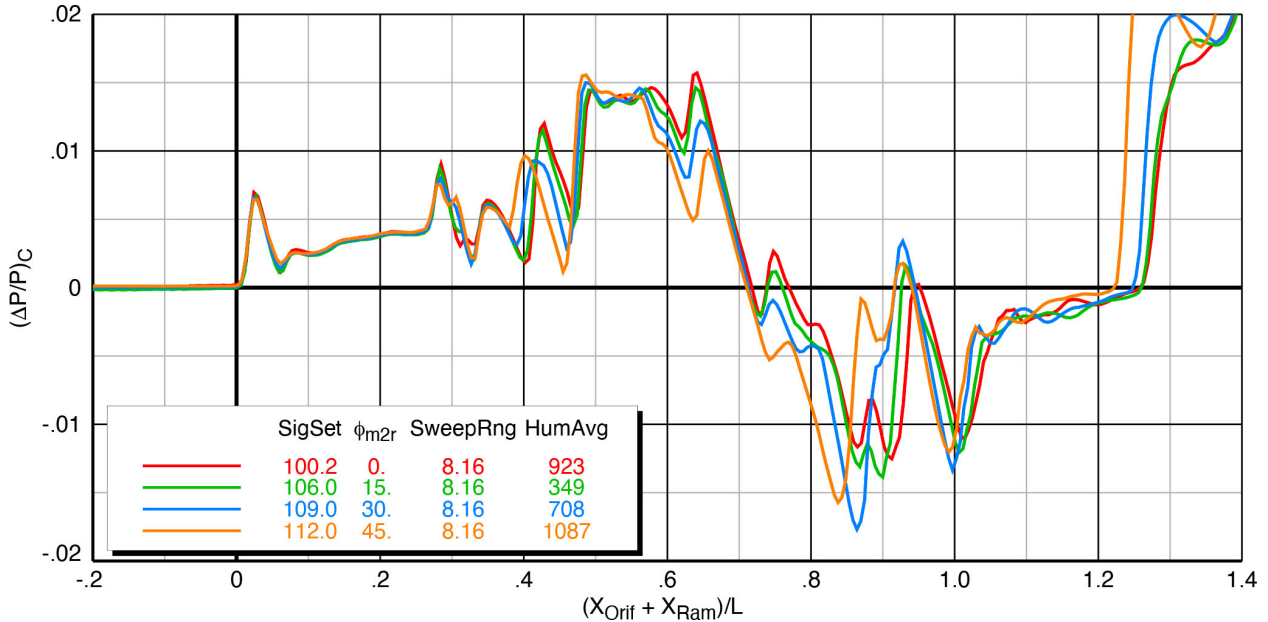

Figure 19 Effect of height on X-59 model (blade strut) spatially-averaged pressure signatures, Mach 1.4, $\alpha = 2.1°$, $\phi_{m2r} = 0°$

19

G. Effect of Roll Angle

The model was set at roll angles from 5° to 45° relative to the pressure rail to assess the changes in the signatures at equivalent off-track angles away from the centerline boom propagation. Figure 20 contains two plots showing the effects of roll angle: the first plot with data at 15° roll increments from 0° to 45°, and the second with 5° increments over the same range. Though the second plot includes the same data as in the first plot, the greater spread among the curves in the first plot makes it easier to see the trends in the signatures as roll angle is increased.

There is a general reduction in pressure levels in the middle part of the signatures as roll angle is increased, but in the aft part, the signature changes are more complicated with all the interactions of the shock waves from the multiple surfaces at the rear of the vehicle.

(a) 15° roll angle increments
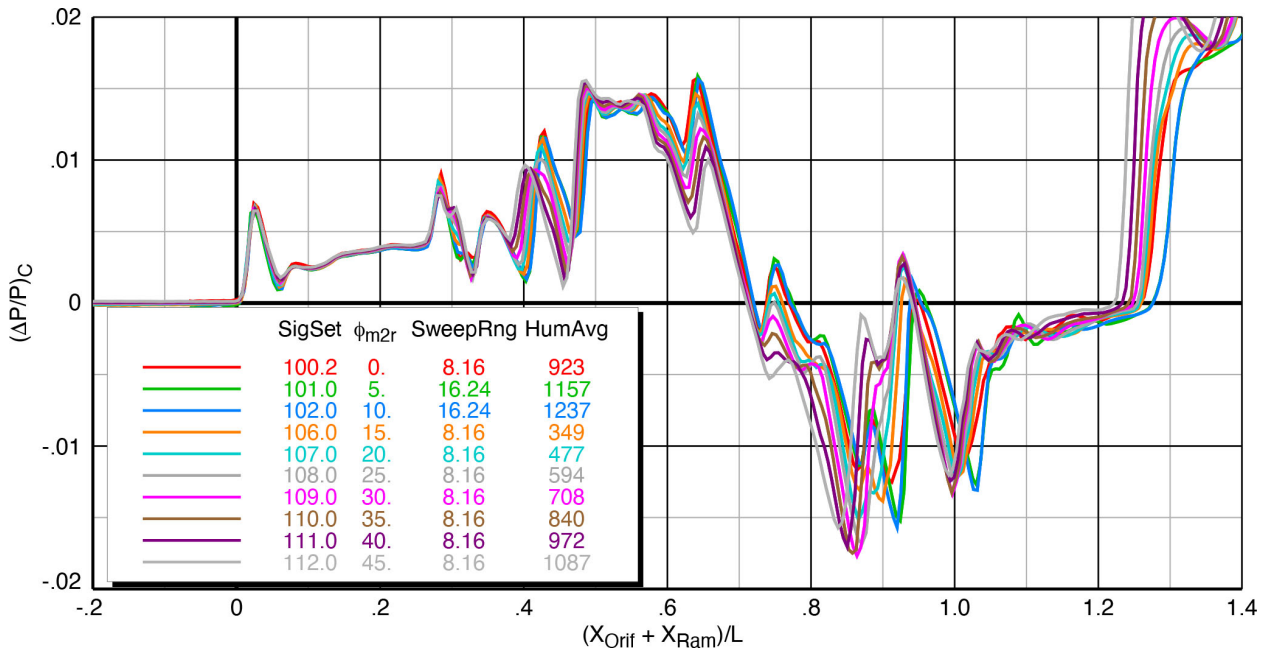
(b) 5° roll angle increments

Figure 20 Effect of roll angle on X-59 model (blade strut) spatially-averaged pressure signatures, Mach 1.4, $h/L = 1.2$, $\alpha = 2.1°$

H. Effect of Mach Number

A plot of Mach number effects on the X-59 signatures is presented in Figure 21. The primary effect of increasing Mach number on a pressure field around an aircraft is to increase the angle of the shock waves away from the vertical. Thus, for a given model position in the wind tunnel, as Mach number is increased, the model shocks fall further aft on the rail. This effect is taken out in the data plots below because the signatures are all aligned with the start of the nose shock being at $X/L = 0$. However, there is also some stretching of the signatures with Mach number, as evidenced in signatures below.
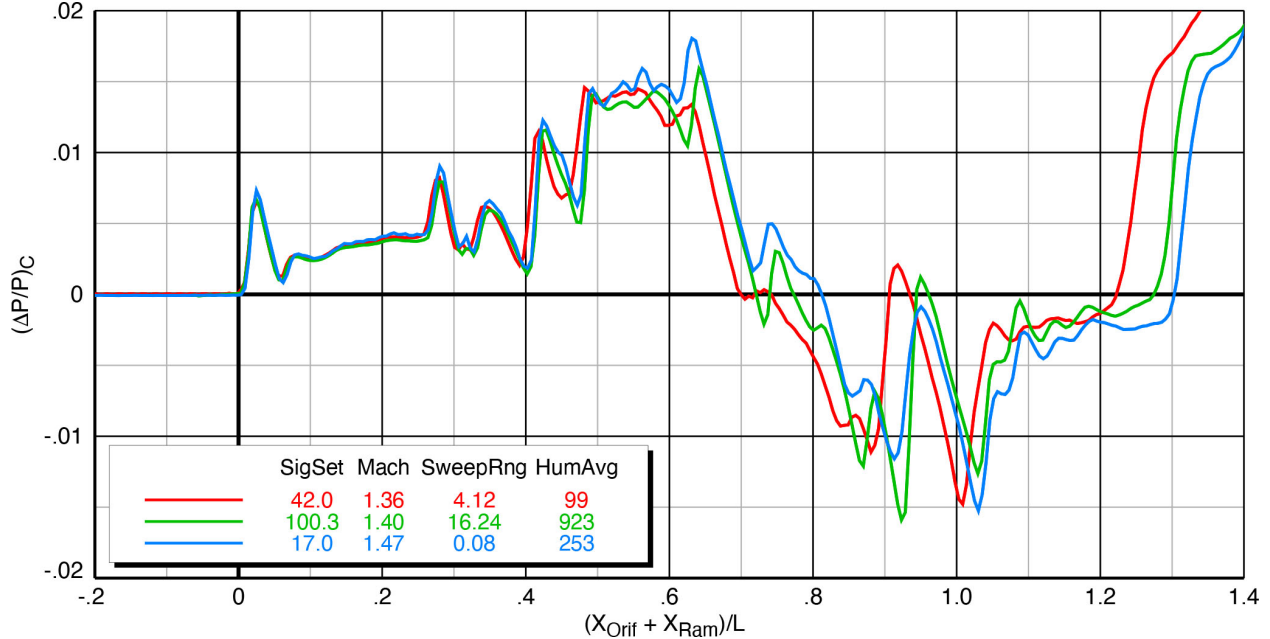

Figure 21 Effect of Mach number on X-59 model (blade strut) spatially-averaged pressure signatures, $h/L = 1.2$, $\alpha = 2.1°$, $\phi = 0°$

I. Blade Strut vs. Sting Mount

Any hardware that is used to support a model in a wind tunnel necessitates a compromise in the outer model line (OML) of the model which adversely affects the aerodynamics of the model and the pressure field surrounding it. A common way to provide data to correct for, or at least partially mitigate these effects, is to test the model with two or more different mounting configurations. For the X-59 sonic boom model, it was decided to design a mount that would attach at the top center of the model so that the aft end would have a clean OML that matches the airplane, as well as a sting mount that attaches through (or in this case, in place of) the engine nacelle so that the upper part of the model is not compromised. Neither configuration provides a complete pressure signature that matches what an airplane would produce in free air, but the combination of the signatures from the two mounting configurations can offer insights into what a composite signature would look like.

A comparison of the signatures for the model mounted on the blade strut vs. the sting is presented in Figure 22. In the plot legend, the model-mounting configuration is specified as either Blade or Sting. The two signatures in the plot are nearly identical up to the shock from the leading edge of the blade strut which falls near $X/L = 0.45$. The pressures fluctuate a bit aft of this point, which are from the flow passing around the strut and interacting with the wing as they pass around to the bottom of the model. The large shock in the X/L range of 0.90 to 0.95 is from the stabilator leading edge, and this is nearly identical between the two configurations. The most notable difference between the signatures is at the aft end: for the blade strut configuration, the pressures ramp up slowly towards the ambient level ($\Delta P/P = 0$) before encountering the strong shock from the transition area near the top of the blade, whereas the sudden growth in the sting area at 2" behind the nozzle exit creates a strong shock that overtakes the rear of the signature at $X/L = 1.03$.
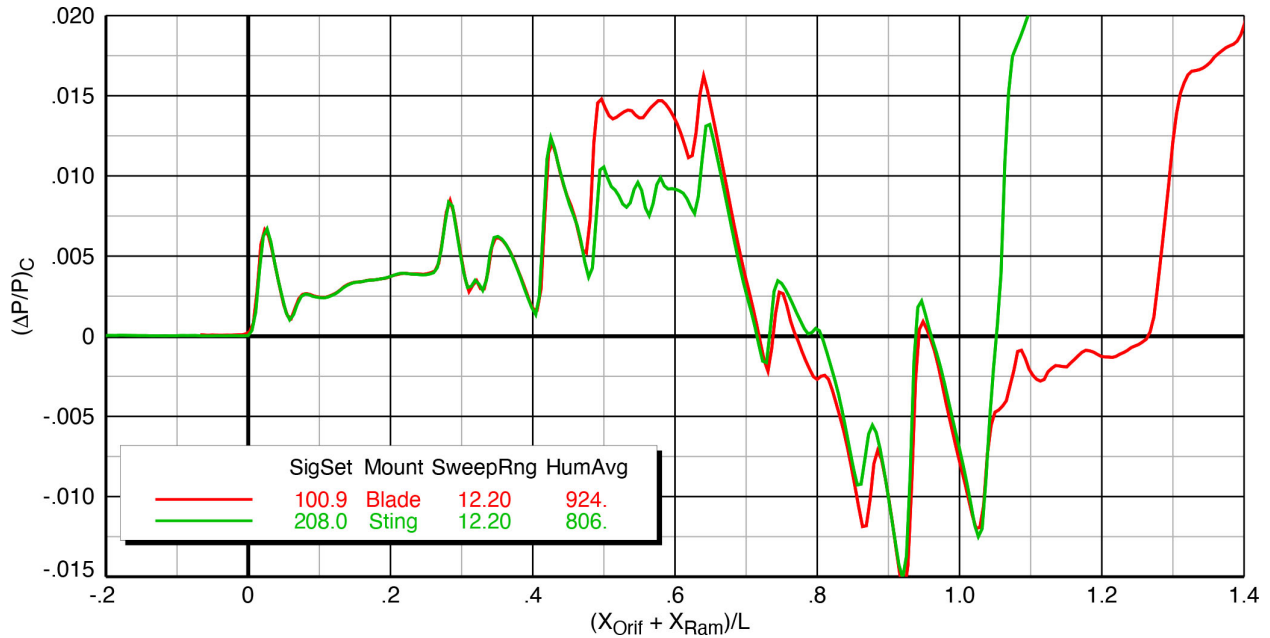
**Figure 22 Comparison of blade strut vs. sting mounts on X-59 model averaged signatures,
Mach 1.4, $h/L = 1.2$, $\alpha = 2.1°$, $\phi = 0°$**

VII. Conclusions

A sonic boom test of a 1.62%-scale model of the X-59 airplane was successfully completed in the Glenn 8- by 6-Foot Supersonic Wind Tunnel in September and October 2021. A total of 196 spatially-averaged pressure signatures were obtained during the 5-1/2 weeks of test time. The signatures provided insight into the near-field sonic boom characteristics of the X-59 at various angles of attack and roll, Mach numbers, and control deflections. Many repeat runs were conducted to assess the quality of the data, and the repeatability was generally very good, though there were at times some unknown influences on the pressure data that compromised some of the signatures. The range of the X sweeps selected within the 24" of available ram extension typically had a very significant influence on the quality of the signatures and the scatter among the runs within a sweep. There was generally less scatter among runs in which the pressures were measured at further-forward locations on the rail, allowing for better repeatability of the averaged signatures.

The data showed clear trends of signature aging over distances of 1.2 to 3 body lengths from the rail. Increments in the shock wave strengths and locations from various control deflections are easily apparent in the rear part of the signature data. Varying the angles of attack and roll, and varying the Mach number, had the expected effect on the signatures.

Humidity varied substantially throughout the test, starting out low (usually less than 100 ppm) at the start of a running shift and often exceeding 1,000 ppm by the end of the shift. However, the data plots consistently showed that even large differences in humidity between averaged signatures did not affect the pressure measurements.

The data from this test will be used in validating CFD codes that are used for sonic boom predictions, and in preparing the data sets that will be used to compare to the signatures measured in flight and on the ground from the X-59 flight tests.

VIII. References

1. https://www.nasa.gov/aeroresearch/programs/aavp/cst

2. https://www.nasa.gov/aeroresearch/programs/aavp

3. Morgenstern, John, Norstrud, Nicole, Sokhey Jack, Martens, S., and Alonso, Juan: "Advanced Concept Studies for Supersonic Commercial Transports Entering Service in the 2018 to 2020 Period", Phase I Final Report, NASA/CR-2013-217820, February 2013.

4. Morgenstern, John, et al: "Advanced Concept Studies for Supersonic Commercial Transports Entering Service in the 2018 to 2020 Period", Phase II Final Report, NASA/CR-2015-218719, July 2015

5. Magee, Todd E., Wilcox, Peter A., Fugal, Spencer R., Acheson, Kurt E., Adamson, Eric E., Bidwell, Alicia L., and Shaw, Stephen G.: *System-Level Experimental Validations for Supersonic Commercial Transport Aircraft Entering Service in the 2018–2020 Time Period, Phase I Final Report.* NASA CR-2013-217797, February 2013

6. Magee, Todd E., Fugal, Spencer R., Fink, Lawrence E., Adamson, Eric E., and Shaw, Stephen G.: System-Level Experimental Validations for Supersonic Commercial Transport Aircraft Entering Service in the 2018–2020 Time Period, Phase II Final Report. NASA CR-2015-218983, November 2015

7. Cliff, Susan E., Durston, Donald A., Elmiligui, Alaa A., Walker, Eric L., and Carter, Melissa B.: *Experimental and Computational Sonic Boom Assessment of Lockheed-Martin N+2 Low Boom Models,* NASA TP-2015-218483, January 2015

8. Durston, Donald A., Elmiligui, Alaa A., Cliff, Susan E., Winski, Courtney S., Carter, Melissa B., and Walker, Eric L.: *Experimental and Computational Sonic Boom Assessment of Boeing N+2 Low Boom Models,* NASA TP-2015-218482, January 2015

9. https://www.nasa.gov/quesst

10. https://www.nasa.gov/image-feature/x-59-wind-tunnel-testing-at-nasa-glenn

11. Durston, Donald A., Wolter, John D., Shea, Patrick R., Winski, Courtney S., Elmiligui, Alaa A., Langston, Sarah L., Bozeman, Michael D., Carter, Melissa B., Ponder, Jonathon D., Heineck, James T., and Bellido, Christopher A.: *X-59 Sonic Boom Test Results from the NASA Glenn 8- by 6-Foot Supersonic Wind Tunnel.* NASA/TM-20220012155, September 2022

12. Carter, Melissa B., Elmiligui, Alaa A., Park, Michael A., Shea, Patrick R., Winski, Courtney S., Durston, Donald A., Jensen, James C., Wagner, Jacob M., Neuhoff, Scott M., and Wolter, John D.: Experimental and Computational Study of the X-59 Wind Tunnel Model at Glenn Research Center 8- by 6-foot Supersonic Wind Tunnel. NASA/TM-20220011496 (to be published in 2022)

13. Soeder, Ronald H.: NASA Lewis 8- by 6-Foot Supersonic Wind Tunnel User Manual, NASA TM 105771, February 1993

14. Castner, Raymond S. and Simerly, Stephanie R.: Assessment of the NASA Glenn 8- by 6-Foot Supersonic Wind Tunnel Supersonic Test Section for Sonic Boom and Supersonic Testing, NASA/TM-20220000420 (to be published in 2022)

15. Magee, Todd E., Shaw, Stephen G., and Fugal, Spencer R.: *Experimental Validations of a Low-Boom Aircraft Design,* AIAA Paper 2013-0646, 51st AIAA Aerospace Sciences Meeting, Grapevine TX, January 2013

16. https://www.nasa.gov/aero/x-59-research-aircraft-overview